1-10-2005

Ultrarelativistic Plasma Shell Collisions in γ-Ray Burst Sources: Dimensional Effects on the Final Steady State Magnetic Field

C. H. Jaroschek
Max-Planck-Institute for Extra- terrestrial Physic

H. Lesch
Max-Planck-Institute for Extra- terrestrial Physic

R. A. Treumann
Dartmouth College

The Astrophysical Journal, 618:822–831, 2005 January 10

ULTRARELATIVISTIC PLASMA SHELL COLLISIONS IN γ-RAY BURST SOURCES: DIMENSIONAL EFFECTS ON THE FINAL STEADY STATE MAGNETIC FIELD

C. H. Jaroschek,[1,2] H. Lesch,[1,2] and R. A. Treumann[1,3]

Received 2004 March 16; accepted 2004 September 3

ABSTRACT

Ultrarelativistic electron-positron plasma shell collisions as an integral part of generic γ-ray burst (GRB) fireball models are studied in the framework of self-consistent three-dimensional particle-in-cell simulations. We compare scenarios at moderately relativistic ($\gamma_0 \simeq 10$) and ultrarelativistic ($\gamma_0 \simeq 100$) energies that directly correspond to the regimes of internal and external shell collisions, respectively, in GRB synchrotron emission models. Simulated systems comprise 5×10^8 particles, applying a relativistic, fully electromagnetic, massively parallelized code. It is found that Weibel-generated, steady state magnetic equipartition ratios in external collisions reach up to $\epsilon_B \sim 12\%$, exceeding the respective internal ratios by nearly a power of 10. Enhanced ϵ_B yields can be explained theoretically by the effective reduction of dimensionality in the ultrarelativistic limit, i.e., the energy-dependent confinement of the three-dimensional Weibel instability within quasi–two-dimensional plasma shell slices.

Subject headings: acceleration of particles — gamma rays: bursts — magnetic fields — plasmas

1. INTRODUCTION

Theoretical concepts of astrophysical phenomena such as extragalactic jets, cosmical magnetic fields, and γ-ray bursts (GRBs) rely on a thorough understanding of relativistic plasma beam instabilities in the highly nonlinear regime. In generic GRB fireball models, a compact central engine ejects electron-positron (e, p) plasma shells (for an extensive review on GRBs, see Piran 1999; Meszaros 2002). To resolve the "compactness problem" (i.e., the optical thickness against pair production at the observed extreme γ-ray luminosities) by means of relativistic beaming, the shells must be confined within a narrow opening angle around the source and move at highly relativistic speeds. Source variabilities cause internal plasma shell collisions at relativistic energies, $\gamma_0^{\rm int} \sim 10$, that are claimed to be responsible for the γ-ray emission via Comptonized synchrotron radiation. GRB radio afterglows can be explained by direct synchrotron emission resulting from the interaction of plasma shells with the external medium at significantly higher collision energies of $\gamma_0^{\rm ext} \sim 100-300$ (Panaitescu & Kumar 2002). The generation of magnetic fields close to equipartition during the shell collisions is essential for all synchrotron emission models. Magnetic field enhancement via shock compression at the boundary of interpenetrating shells is one option proposed (Kazimura et al. 1998), although the rapid decay of the magnetic field strength behind the shock front represents a systematic weakness (Gruzinov 2001) of this model. The approach by Medvedev & Loeb (1999) and Pruet et al. (2001) of magnetic field generation via the Weibel instability (Weibel 1959), which is effective in the counterstreaming plasmas of deeply interpenetrating colliding shells, appears to be extremely promising. We note that the term "collision" refers to the interaction between rarefied plasmas of different bulk motion (=shells), within which the charged particles experience scattering at the collective fields of plasma instabilities (Sagdeev 1966). The validity of the Weibel approach with respect to magnetic field generation has been confirmed in particle-in-cell (PIC) simulations of colliding (e, p) plasma shells at weakly to moderately relativistic collision energies $\gamma_0^1 = 1.17$ and $\gamma_0^{10} = 10.05$ (Silva et al. 2003), which applies to the regime of internal collisions. Therein, final steady state equipartition ratios of the magnetic field energy $\epsilon_B \sim 0.25\%$ (2.5%) for γ_0^1 and γ_0^{10}were obtained. The equipartition ratio ϵ is defined as the ratio of field to the total particle relativistic energy. In the present article we report three-dimensional PIC simulation results on the magnetic field generation by the electromagnetic (EM) counterstreaming instability at external collision energies of $\gamma_0^{100} = 100.005$. In three-dimensional scenarios, the EM counterstreaming instability (Haruki & Sakai 2003; Saito & Sakai 2004) is a two-dimensional coupled two-stream Weibel (CTW) mode. For comparison, we reproduce shell collisions at the moderate γ_0^{10}, and can confirm the results of Silva et al. (2003). We show that at external collision energies of γ_0^{100}, even higher equipartition magnetic field ratios up to $\epsilon_B \sim 12\%$ are obtained. In contrast to the internal case, magnetic fields in the saturation and final steady state phases become comparable. In the present analysis we focus on the behavior of the two-dimensional CTW mode as a function of collision relativistic energy. Therefore, plasma shells are initially cold to avoid kinetic contributions of finite thermal spread within the linear regime. However, the Weibel mode is an inherently kinetic instability (Weibel 1959) and the scenario of counterstreaming plasmas is nothing else but an extreme form of temperature anisotropy. Therefore, we present a thorough discussion of the limits of the cold plasma approximation and the effects of nonnegligible thermal spread, and define the characteristic quantities affecting the impact of kinetic modifications in the relativistic regime. The energy dependence of equipartition yields in the final steady state configuration indicates that the nonlinear coupling between the unstable Weibel and two-stream modes is sensitive to the transition from moderately relativistic ($\gamma_0^{10} \sim \gamma^{\rm int}$) to ultrarelativistic ($\gamma_0^{100} \sim \gamma^{\rm ext}$) collision energies. Linear stability theory provides good arguments for explaining the energy dependence of the coupled mode, which are subsequently

[1] Center for Interdisciplinary Plasma Science, Max-Planck-Institute for Extraterrestrial Physics, Giessenbachstrasse, Garching 85748, Germany; cjarosch@mpe.mpg.de, tre@mpe.mpg.de.

[2] Observatory of the Ludwig-Maximilians University, Scheinerstrasse 1, Munich 81679, Germany; lesch@usm.uni-muenchen.de.

[3] Department of Physics and Astronomy, Dartmouth College, Hanover, NH 03755.

TABLE 1
Simulation Characteristic Quantities

Simulation	$L_x \times L_y \times L_z$	$u_{z0,1}$	$v_{\mathrm{th},\perp}^{\mathrm{cms}}$
1.....	$25.6 \times 25.6 \times 12.8$	10.00	4.5×10^{-5}
2.....	$25.6 \times 25.6 \times 12.8$	10.00	100.0×10^{-5}
3.....	$25.6 \times 25.6 \times 12.8$	100.00	4.5×10^{-5}
4.....	$51.6 \times 3.2 \times 51.6$	100.00	4.5×10^{-5}

validated in the nonlinear regime at later times by means of the PIC simulations. The essential point is the progressive dominance of the Weibel over the two-stream contributions in the CTW mode at ultrarelativistic energies, causing an energy-dependent reduction of the dimensionality. For extreme collision energies the three-dimensional CTW mode propagates in quasi–two-dimensional shell slices transverse to the bulk motion. We finally conclude that the reduced dimensionality in external shell collisions enhances the Weibel-generated magnetic equipartition ratio by 1 order of magnitude.

2. SIMULATION DESCRIPTION

The simulations are performed with a massively parallelized, relativistic, and fully electromagnetic PIC code. A detailed discussion of the PIC method is found in Birdsall & Langdon (1991). The field quantities are represented on a highly refined grid mesh with resolution $\Delta_{x,y,z} = 0.1(c/\omega_{p0})$ in each Cartesian direction. Times are normalized to the inverse plasma frequency $\omega_{p0}^{-1} = (4\pi e^2 n_0/m)^{-1}$, lengths are normalized to the plasma skin depth (c/ω_{p0}) and, consequently, velocities are normalized to the speed of light c. Here e and m are electronic charge and mass, respectively. We study the Weibel instability in three dimensions with a total ensemble up to 5×10^8 individual particles. In the initial configuration, particles are homogeneously distributed in configuration space and appendant to counterstreaming ensembles in velocity space: an upward-moving pair plasma shell $v_{z0,1} > 0$ with electron/positron density $n_{p0} = n_{e0} = n_0$ and an equally dense counterstreaming shell $v_{z0,2} = -v_{z0,1}$. The grid mesh frame is the Lorentzian laboratory and center of mass (cms) frame. Consequently, the system is initially charge and current neutral. The initial setup corresponds to the situation of interpenetrating plasma shells studied in slab geometry, i.e., the conditions prevalent in three-dimensional collisionless shocks in a cms frame comoving downstream of the shock front. A selection of four simulations is presented: two simulation runs at moderately relativistic normalized bulk momentum $p_{z0}/mc = u_{z0} = \gamma_0^{10} v_{z0} = 10.00$ and two simulations runs at ultrarelativistic normalized bulk momentum $\gamma_0^{100} v_{z0} = 100.00$. The different relativistic energies γ_0^{10} and γ_0^{100} not only probe the regimes of internal and external collision energies by direct numerical simulation but also provide insight into the energy dependence of the coupling term in the two-dimensional two-stream Weibel coupled instability for the highly nonlinear evolution at later times. Table 1 summarizes the key quantities of the individual initial setups. Particles are inserted in momentum space according to an isotropic Maxwellian in the comoving frame of the shells. In the cms (=lab) frame, the particle distributions appear to be Lorentz boosted. The finite temperature of the respective Lorentz-boosted Maxwellian corresponds to a thermal velocity spread $v_{\mathrm{th},\perp}^{\mathrm{cms}}$ perpendicular to the bulk motion. We adopt the definition employed in Silva et al. (2003) and Medvedev & Loeb (1999) and define the initial bulk motion in $+z$ as the parallel direction of reference. This is opposite to the convention used in Yoon & Davidson (1987a, 1987b) and Yang et al. (1993a, 1993b), in which the one-dimensional Weibel mode has been analyzed in the presence of a magnetic field providing the preferred direction of parallel propagation. In all simulations that follow, the initialized plasma shells are cold, i.e., the initial perpendicular temperatures $T_\perp$ reside in the electron-volt regime. This situation is fundamentally different from fast-ignitor scenarios. The relativistic definition of temperature and kinetic modifications introduced in the case of significant thermal spread are discussed in § 3.2. For γ_0^{10}, two scenarios are compared that differ by a factor of $\sim$500 in the initial $T_\perp$ in order to put constraints on the validity of the cold beam assumption in the linear stability analysis in § 3.1. Although the plasma shells are cold at initialization and during the linear regime, a fully kinetic numerical plasma model is essential to include nonthermal heating/particle acceleration during later times. The two ultrarelativistic runs are performed in different geometries of the simulated volume to gain insight into the effect of the finite size of the simulation box imposed by computational limitations. We note that the CTW instability is an inherently three-dimensional problem: although the coupled plasma mode is two-dimensional in the linear regime, in the phase of nonlinear saturation only oppositely aligned current self-pinches are mutually neighboring in any two-dimensional plane that includes the z-direction. A third dimension is required to allow for the coalescence of similar current filaments by circumventing the respective countercurrents, as was recognized by Lee & Lampe (1973). The late-time evolution is studied in simulations 1, 2, and 3, which lasted for $\Delta t\omega_{p0} = 260$, requiring 5500 time steps for γ_0^{10} and 45,000 time steps for γ_0^{100} in order to ensure an energy stability of 0.1% and 1%, respectively.

3. DIMENSIONAL EFFECTS IN RELATIVISTIC PLASMA SHELL COLLISIONS

3.1. *Linear Progenitors of the Preeminent Plasma Instability Modes*

In three-dimensional scenarios of counterstreaming plasma shells, the conversion of collision kinetic energy into electromagnetic energy is conducted by the two-dimensional CTW instability. In the linear regime, the system is degenerate in the transverse direction. As already noted, the configuration becomes three-dimensional during nonlinear saturation and coalescence of the current filaments. The CTW instability propagates at oblique angles as the coupled mode consisting of the purely one-dimensional electromagnetic Weibel instability (WBI), which propagates exactly transversely, and the one-dimensional electrostatic two-stream instability (TSI) propagating longitudinally. In all parameter regimes, plasma shell collisions proceed in three successive phases: the linear growth phase, followed by the highly nonlinear saturation phase of the individual modes and the phase of formation of a final steady state configuration. Although the linear phase evolves on timescales/perturbation scale heights irrelevant in the astrophysical context, all the preeminent dissipation channels of the system's free energy are excited. Hence, the linear analysis provides essential interpretative insights into the energy dependence of the linear mode. It also has some predictive power for the processes vital during the two late-time phases, when the nonlinear coupling and kinetic effects come into play.

In the initial setup, the finite thermal spread of plasma shells is negligible. As is shown in § 3.2, the perpendicular temperatures remain in the sub keV regime during the entire linear phase up to the time of nonlinear mode saturation. Consequently,

for the initial setups presented in this article the cold beam approximation is valid for the entire linear regime. The plasma dynamics of counterstreaming (e,p)-shells in the cold beam limit (Califano et al. 1997; Kazimura et al. 1998) is governed by the set of equations consisting of the Lorentz force equation

$$\partial \boldsymbol{p}_i/\partial t + \boldsymbol{v}_i \cdot \nabla \boldsymbol{p}_i = \pm(\boldsymbol{E} + \boldsymbol{v}_i \times \boldsymbol{B}), \tag{1}$$

the dynamic Maxwell equations

$$\partial \boldsymbol{B}/\partial t = -\nabla \times \boldsymbol{E}, \tag{2}$$

$$\partial \boldsymbol{E}/\partial t = \nabla \times \boldsymbol{B} - \sum_i \boldsymbol{j}_i, \tag{3}$$

with the current in each individual shell i given by $\boldsymbol{j}_i = n_{p,i}\boldsymbol{v}_{p,i} - n_{e,i}\boldsymbol{v}_{e,i}$, and the continuity equations

$$\partial n_i/\partial t = -\nabla \cdot \boldsymbol{j}_i. \tag{4}$$

Linearization yields the dispersion relation

$$(1 - 2\Omega_2^{-2})[k_z^2(1 + 2\Omega_4^{-2}) - \omega^2(1 - 2\Omega_1^{-2}) - 4\omega k_z \Omega_3^{-2}] + k_x^2[(1 - 2\Omega_1^{-2})(1 + 2\Omega_4^{-2}) + 4\Omega_3^{-4}] = 0, \tag{5}$$

which contains the dimensionless expressions

$$\Omega_1^{-2} = \sum_i \frac{n_{0,i}}{\gamma_{0,i}\Omega_i^{-2}}, \quad \Omega_2^{-2} = \sum_i \frac{n_{0,i}}{\gamma_{0,i}^3\Omega_i^{-2}}, \tag{6}$$

$$\Omega_3^{-2} = \sum_i \frac{n_{0,i}v_{0,i}}{\gamma_{0,i}\Omega_i^{-2}}, \quad \Omega_4^{-2} = \sum_i \frac{n_{0,i}v_{0,i}^2}{\gamma_{0,i}\Omega_i^{-2}}, \tag{7}$$

where the summation over (e, p)-species has already been performed. Therein, $i = 1, 2$ indicate quantities of the respective shells, i.e., reduced frequency $\Omega_i = \omega - k_z v_{0,i}$ and relativistic energy $\gamma_{0,i} = (1 - v_{0,i}^2)^{-1/2}$. Equation (5) is the dispersion relation of the coupled two-dimensional CTW mode; its lower dimensional constituents are retained in the limits $k_{x,z} \to 0$. In a formal way, the dispersion relation is constituted by the TSI and WBI contributions, which are connected via a coupling term (CT):

$$\mathrm{CTW} = \mathrm{TSI} \times \mathrm{CT} + \mathrm{WBI}. \tag{8}$$

Figure 1 compares the essential information on the linear theory for the weakly relativistic $\gamma_0^1 = 1.17$ (*gray*) with the moderately relativistic and ultrarelativistic regimes $\gamma_0^{10} = 10.05$ and $\gamma_0^{100} = 100.005$ (*dotted and solid lines, respectively*). The WBI mechanism relies on the fact that comoving particles of like charge in one shell, as well as the respective pendant of opposite charge in the counterstreaming shell, represent like currents mutually attracting each other. Incipient neutral-charge current filaments evolve, each sustaining a toroidal magnetic field that self-pinches its generating current and hence closes the instability feedback loop. Self-pinching in colliding (e, p)-shells is limited only by the transverse oscillations of the particles in the Weibel magnetic fields (meandering motion, as directly illustrated by an ensemble of trace particles in Fig. 4*b*). The central idea of "dimensional effects" is based on the energy dependence of the two-dimensional CTW mode in the highly relativistic regime (i.e., $\gamma_0 \geq 5$), which is understood as the superposition of its one-dimensional constituents. In Figure 1*a*, the growth rates Γ_{WBI} of the purely transverse one-dimensional WBI are shown. In the cold-beam limit, the WBI has a finite growth rate at all wavelengths of interest for the weakly relativistic to ultrarelativistic regimes. At high relativistic energies, Γ_{WBI} scales as $\Gamma_{\mathrm{WBI}} \propto \gamma_0^{-1/2}$ as a function of collision energy. Relativistic damping is much more severe for the one-dimensional TSI mode as the purely longitudinal constituent. It evolves from Langmuir fluctuations driven by the relative motion of the shells. Here $\Gamma_{\mathrm{TSI}} \propto \gamma_0^{-3/2}$ directly images the behavior of the maximum of the TSI growth rate as shown in Figure 1*b*, as well as the cutoff shift toward longer wavelengths. The value of Γ_{TSI} drops by a factor of $\sim 100^{3/2}$ from ~ 0.63 to $\sim 7.1 \times 10^{-4}$ during the $\gamma_0^1 \to \gamma_0^{100}$ transition. Consequently, mode damping due to relativistic mass gain is much more severe for the direction parallel rather than perpendicular to the shells' bulk motion. The relativistic energy dependence is retained in a straightforward manner if the momentum variations $\delta p_\perp = \gamma_0 \delta v_\perp$ (WBI) and $\delta p_\parallel = \gamma_0^3 \delta v_\parallel$ (TSI) in the respective directions are considered. Variations in the fields act via the Lorentz force (eq. [1]) on the momentum variations, which then transfer to velocity variations according to the relativistic bulk motion as a preferential, nondegenerate direction. Variations in velocity introduce variations in density/currents by continuity (eq. [4]), closing the feedback loop to the fields (eqs. [2] and [3]). Besides the coupling term, the TSI and WBI contributions to the CTW are biquadratic, hence $\Gamma_{\mathrm{WBI}} \propto \gamma_0^{-1/2}$ and $\Gamma_{\mathrm{TSI}} \propto \gamma_0^{-3/2}$ are motivated. The behavior of the two-dimensional CTW mode results from the superposition of its one-dimensional components. The maximum growth of TSI and WBI are comparable in the non- and weakly relativistic regimes (Figs. 1*a* and 1*b*). Both modes show significant differences in energy scaling. As a consequence, the relative weights of the respective contributions and the total coupling strength in the two-dimensional CTW exhibit a strong dependence on relativistic energy. The relative weight of each contribution is reflected in the propagation angle, which migrates to the quasi transversal for $\gamma_0 \to 100$ (Fig. 1*c*). The cutoff is retained from the TSI and is always present in the two-dimensional mode (Fig. 1*d*). The cutoff in the (k_x, k_z)-plane is sharp, while the growth rate is practically flat within the unstable region at $\Gamma_{\mathrm{CTW}}^{100}/\omega_{p0} = 0.14$ and $\Gamma_{\mathrm{CTW}}^{10}/\omega_{p0} = 0.51$ for $\gamma_0 = 100$ and 10, respectively. The dashed lines in Figure 1*d* indicate the (k_x, k_z)-space that is covered by the finite grid resolution/box extension in the PIC simulation as imposed by the computational limitations. The coupling strength weakens significantly, since Γ of the WBI becomes comparable to the CTW mode for $\gamma_0 \to 100$, and hence decoupling sets in earlier in this limit. In all modes, the source of free energy is the bulk kinetic energy of the shells. The propagation angle of the fastest-growing two-dimensional mode turns abruptly into a quasi-perpendicular direction, reflecting the dominance of the WBI over the TSI in the coupled mode. In conclusion, for relativistic collision energies beyond $\gamma_0 \sim 30$ the physics of an initially three-dimensional shell configuration ultimately takes place within two-dimensional plane-parallel shell slices (which in particular is valid in the linear regime), i.e., the transition to the ultrarelativistic regime implies an effective reduction in dimensionality. The validity and implications of this statement are investigated in § 3.3 in PIC simulations of the highly nonlinear late-time evolution of the system.

3.2. *Effects of a Finite Thermal Spread: Kinetic Modifications*

The Weibel instability is an inherently kinetic instability (Weibel 1959; Yoon 1989) with the temperature anisotropy

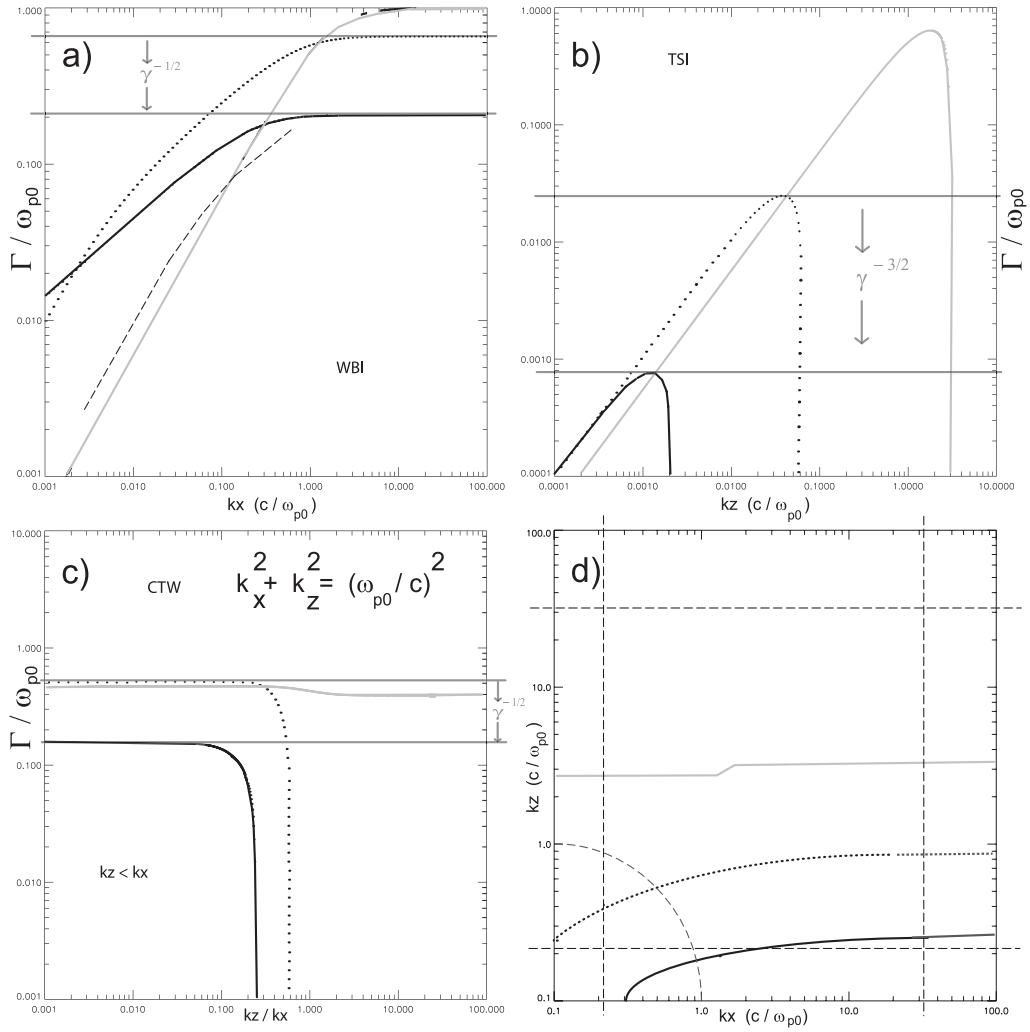

FIG. 1.—Linear growth rates (*a*) $\Gamma(k_x)$ of the one-dimensional WBI, (*b*) $\Gamma(k_z)$ of the one-dimensional TSI, and (*c*) $\Gamma(k_z/k_x)$ of the two-dimensional CTW mode (the latter taken on the dashed circle of constant k as indicated in [*d*]) for different collision energies γ_0^1, γ_0^{10}, and γ_0^{100} (*gray, dotted, and solid lines*). For comparison, in (*a*) the Yang et al. (1993b) growth rate for the "double waterbag distribution" is given (*dashed line*). From (*a*)–(*c*), it is obvious that in the ultrarelativistic regime the WBI contributions to the two-dimensional CTW dominate over the respective TSI contributions. Consequently, the two-dimensional CTW appears to propagate in an almost perpendicular direction $k_z/k_x \ll 1$. The value of $\Gamma(k_z/k_x)$ is near constant at unstable angles and exhibits sharp angular cutoffs. (*d*) Cutoff wave vectors $k^1_{\max}$, $k^{10}_{\max}$, and $k^{100}_{\max}$ for the CTW in (k_x, k_z)-space. Dashed straight lines give the Fourier limits imposed by the grid resolution/box extension, indicating that the unstable regions are well resolved numerically in all energy regimes.

$\Delta_T = T_\parallel/T_\perp - 1$ as the driving source of free energy. Each counterstreaming plasma shell represents an intense plasma beam. A plasma beam of finite thermal spread is the limiting case of strong T-anisotropy. In the relativistic regime, temperatures parallel ($T_\parallel$) and perpendicular ($T_\perp$) to the bulk motion $v_0\,\boldsymbol{e}_z$ are coupled via the relativistic $\gamma_0 = (1 - v_0^2)^{-1/2}$ in the energy-momentum tensor $T^{\sigma\sigma}$ (de Groot et al. 1980). The spatial components in covariant form, $T^{mn}/mc^2 = \int d^3p u^m v^n f(\boldsymbol{p})(m, n = 1, 2, 3)$, constitute the temperature tensor in the most general formulation as the second moment of the normalized distribution function $f(\boldsymbol{p})$. Assuming that the anomalous resistivity is negligible during the linear regime and accounting for a symmetric degeneracy in the perpendicular direction, T^{mn} reduces to the diagonal elements

$$T_\perp/mc^2 = \frac{1}{2}\int d^3p u_\perp v_\perp f(p_\perp, p_\parallel) \tag{9}$$

and

$$T_\parallel/mc^2 = \int d^3p u_\parallel v_\parallel f(p_\perp, p_\parallel). \tag{10}$$

Consequently, for a given perpendicular thermal spread $v_{\mathrm{th},\perp}$ the relativistic collision energy γ_0 determines the significance of thermal effects. Two questions arise in the present study: (1) Which thermal effects are predicted by linear kinetic theory and in which parameter regime of the critical quantities γ_0 and Δ_T will such effects become important? (2) What consequences result for the argumentation given in § 3.1?

The purely transverse relativistic Weibel instability has been studied kinetically in the context of "waterbag" models (Yoon & Davidson 1987a, 1987b; Yang et al. 1993a, 1993b; Silva et al. 2002). The characteristic of such models is to approximate the finite thermal spread by a step-functioned particle distribution,

$$F(\boldsymbol{p}, \boldsymbol{p}_{\mathrm{th}}) = \theta(\boldsymbol{p}_{\mathrm{th}}^2 - \boldsymbol{p}^2), \tag{11}$$

in order to simplify the linear kinetic analysis. (We note that in the one-dimensional studies by Yoon & Davidson [1987a, 1987b] and Yang et al. [1993a, 1993b], the Weibel instability defines the direction of parallel propagation.) Since the Weibel mode propagates transverse to the bulk motion, the definitions

of parallel and perpendicular are exactly interchanged compared with those used in this article and by Medvedev & Loeb (1999) and Silva et al. (2002, 2003). Yoon & Davidson (1987b) and Silva et al. (2002) considered a single waterbag distribution to investigate the effect of a finite $T_\perp$, i.e., a finite thermal spread in the direction of Weibel propagation. By assuming a ring distribution in the plane of momentum space that is normal with respect to the waterbag, Yoon & Davidson (1987b) introduced a large initial anisotropy. Within this plane the absolute momenta are sharply δ-confined, and zero bulk momentum is ensured by the circular symmetry. Linear stability analysis then shows that in the relativistic regime kinetic effects produce an upper cutoff for the unstable wavenumbers; i.e., short-scale Weibel fields are inhibited and the Weibel instability can develop only on sufficiently large spatial scales, retaining the $\Gamma_{\rm WBI} \propto \gamma_0^{-1/2}$ behavior. However, the constraints on spatial scales and growth rate depend critically on the T-anisotropy, Δ_T. For a sufficiently large Δ_T, every criterion for an upshift in the wavenumber cutoff is met. For instance, an initial $\Delta_T \geq 10$ guarantees mode growth within the constraints of our simulation box even for γ_0^{100}. Silva et al. (2002) substituted a particle beam for the ring in momentum space. As in Yoon & Davidson (1987b), the instability is carried by electrons within an immobile charge-neutralizing background. Silva et al. (2002) further introduce an ensemble of background electrons that imposes some constraints on the relative beam strength, $\chi = n_0/n_{\rm bgd}$. In the ultrarelativistic regime this scenario is close to the configuration of counterstreaming shells. The essentials of the analysis by Silva et al. (2002) are the threshold conditions for Weibel growth in χ and $T_\perp$. Since the initial beam spread $\sigma_{\rm sp} \lesssim 10^{-8}$ and the two-stream limit $\chi \sim 1$ are valid, the threshold condition $\chi \geq \gamma_0 v_{\rm th}^2/v_0^2 = \sigma_{\rm sp}$ is fulfilled in all our simulations with no restriction. Severe damping of Weibel growth in the strong beam limit is observed for $T_\perp \geq 50$ keV. Such limiting constraints on Weibel growth are important for the fast-ignitor scenarios, in which the beam is usually density rarefied, and in plasma shell collisions, in which the thermal spread amounts to at least $\sim$1% of the bulk momentum. Moreover, Yang et al. (1993b) extend the sharp plasma beam to a second waterbag distribution, $G(p_\parallel) = \theta(p_0^2 - p_\parallel^2)$, with $p_0/mc = (\gamma_0^2 - 1)^{1/2}$, in order to investigate the effects of a parallel close-to-thermal velocity spread. The analysis contains the effect of a magnetic field parallel to the direction of Weibel propagation. However, some central insights are retained into the limit of negligible magnetic field strength. In the regime of dominant $T_\parallel$ (which is always the case in shell collisions with dominant bulk motion), the stability properties are determined by the relative weight of the $T_\perp$-contributions, i.e., by Δ_T. In the limit $T_\perp \to 0, \Delta_T \to \infty$ (see dashed line in Fig. 2*a* of Yang et al. 1993b), the WBI mode is purely growing over a broad range of wavenumbers. The quantitative growth rate is consistent with $\Gamma_{\rm WBI}$ computed for a cold plasma beam (see Fig. 1*a* dashed line for comparison). Consequently, for an extreme Δ_T the waterbag and beam models become indistinguishable. As observed by Silva et al. (2002), for the beam distribution the extension to finite $T_\perp$ causes an upper cutoff in the wavenumber region of Weibel growth for the model distribution used by Yang et al. (1993b). The cutoff scales as

$$k_{\rm cut}(c/\omega_{p0}) = (2\pi/3\gamma_0)^{1/2}\Delta_T, \tag{12}$$

which implies that for sufficiently high Δ_T the growth of Weibel modes extends into the range of short wavelengths. To be more precise, the above threshold value was derived by Yang et al. (1993b) using a Nyquist analysis of a so called smooth distribution function, which had been designed to model a power-law distribution at high energies. However, differences between smooth and waterbag distributions become insignificant at large Δ_T. Thus, the critical quantities determining the importance of kinetic effects in relativistic plasma shell collisions are the collision energy γ_0 and the temperature anisotropy Δ_T. Figures 2*a*–2*c* show the time evolution of $T_\perp, T_\parallel$, and Δ_T as computed in the fully self-consistent PIC simulations. The initial $T_\parallel$ is given by the relativistic collision energy γ_0. For the cold initial perpendicular temperatures at hand, the Maxwellian velocity spread as shown in Table 1 per definitionem corresponds to $T_\perp/mc^2 = v_{\rm th,\perp}^{\rm cms2}$. Such conditions are well modeled by the waterbag distribution in equation (11), for which one obtains

$$T_\parallel/mc^2 = \gamma v_0^2 \xi(v_{\rm th,\perp}^{\rm cms}) \tag{13}$$

and

$$T_\perp/mc^2 = \frac{1}{2}\gamma[1 - \xi(v_{\rm th,\perp}^{\rm cms}) + v_{\rm th,\perp}^{\rm cms2}\xi(v_{\rm th,\perp}^{\rm cms})], \tag{14}$$

with $\xi(x) = 1/2x \ln[(1+x)/(1-x)]$. In the limit of small thermal spread, $v_{\rm th,\perp}^{\rm cms} \ll 1$ and $\xi(x) \simeq 1 + x^2/3 + \ldots$, one obtains

$$\hat{T}_\parallel/mc^2 = \gamma_0, \qquad \hat{T}_\perp/mc^2 = \frac{1}{3}\gamma_0 v_{\rm th,\perp}^{\rm cms2}. \tag{15}$$

For simulations 1, 3, and 4, the values $\hat{T}_\perp/mc^2 = 6.8\times10^{-8}$ are close to the Maxwellian $T_\perp/mc^2 = 2.0\times10^{-7}$. Comparison with the time evolution of the equipartition ratios in Figure 2*d* shows that at the respective collision energies γ_0^{10} and γ_0^{100}, throughout the linear instability regime the perpendicular temperatures are in the sub-keV domain and the corresponding anisotropy ranges well above $\Delta_T \geq 10^4$. Consequently, the transversal cutoffs caused by finite $T_\perp$ are expected to occur at $k_{x/y,\rm cut}(c/\omega_{p0}) \sim 10^4$. Such values are far beyond the smallest spatial scales of interest in the astrophysical context, since in the nonlinear regime the instability migrates toward larger scales anyway. We note that the estimates of the kinetic contributions are based on a one-dimensional linear analysis. However, the idea is to point out in which parameter regime modifications due to kinetic effects could be expected, of what kind these modifications are, and by which critical quantities they are controlled. The values of $T_\parallel$ and Δ_T obtained from the PIC data indicated that the assumption of negligible thermal spread for the linear analysis in § 3.1 is well justified in our simulations. To provide additional evidence that the above estimates can be transferred to the two-dimensional CTW case, additional simulations are performed with energies γ_0^{10} and γ_0^{100} (Table 1). At γ_0^{10}, simulations 1 and 2 differ by a factor of $\sim$500 in the initial $T_\perp$ and Δ_T. Since the limit $\Delta_T \to \infty$ applies to both runs, the time evolution in Figures 2*a*–2*c* and 3*a* is comparable. Furthermore, the difference in initial $T_\perp$ and Δ_T is negligible even beyond the linear regime up to the phases of nonlinear saturation and the final steady state. In the γ_0^{100} cases (simulations 3 and 4), transverse and longitudinal extensions of the simulation box have been varied in order to investigate any possible effects of the finite size of the computational domain on linear mode growth. This has been done for the higher energy because limitations in the range of unstable wavenumbers are then expected to be more severe, keeping in

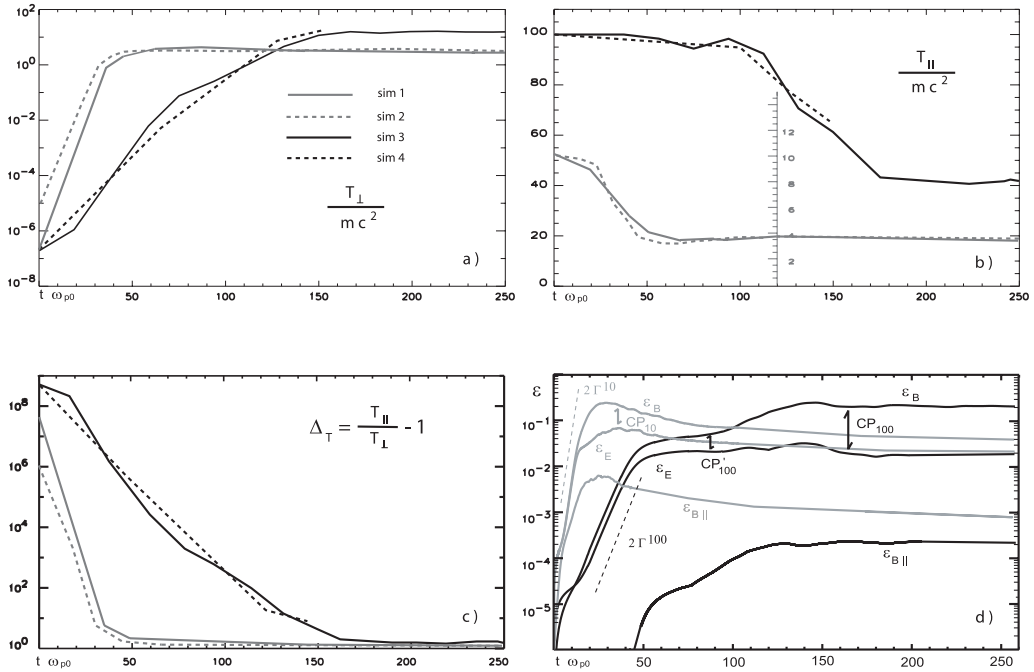

FIG. 2.—(*a*) Time evolution of perpendicular temperature $T_\perp$ for γ_0^{10} (*gray*) and γ_0^{100} (*black*). During linear mode growth (cf. [*d*]), $T_\perp < 1$ keV. Thus, for all simulations (see simulation 2: *dashed gray line*) variations in $T_\perp$ are insignificant and the cold beam limit applies. The final state is also independent of the initial thermal spread for the cold initialization at hand. (*b*) Time evolution of $T_\parallel$ (line coding as in [*a*]; note the expanded scale for the run with γ_0^{10}!). In the linear regime, $T_\parallel$ is dominated by the bulk motion; therefore, waterbag and beam distributions yield comparable results. At later times, significant beam energy is deposited in Weibel electromagnetic fields and particle heating. The resulting temperature anisotropies of $\Delta_T \geq 10^4$ (*c*) for the respective runs during the linear regime clearly indicate that thermal-mode damping or restrictions to the range of unstable wavenumbers are negligible. Remarkably, a finite residual anisotropy $\Delta_T \sim 2-3$ remains. The time evolution of equipartition ratios is given in (*d*) for γ_0^{10} (γ_0^{100}) (*gray* [*black*]), with linear growth up to $t_1\omega_{p0} = 13(42)$, saturation at $t_2\omega_{p0} = 27(145)$, and the final steady state at $t_3\omega_{p0} > 130(190)$. The coupling strength in the two-dimensional CTW mode weakens from γ_0^{10} toward γ_0^{100}, i.e., $CP_{10} > CP_{100}$. The contributions of $B_\parallel$ are persistently negligible. In general, longitudinal modifications to the total field configuration, which are attributed to TSI, are prominent only at γ_0^{10}.

mind the results of the linear kinetic analysis discussed above. Figures 2*a*–2*c* and 3*b*, as well as the analysis of the late-time nonlinear evolution in § 3.3, demonstrate that no such restrictions apply to our simulations. Even more convincing evidence that thermal effects play no role in the present study is the comparison of the analytic growth rates with the growth rate determined from the PIC results in the linear regime. Linear growth rates (§ 3.1) for the two-dimensional coupled CTW mode of $\Gamma_{\rm CTW}^{100}/\omega_{p0} = 0.51$ and $\Gamma_{\rm CTW}^{10}/\omega_{p0} = 0.14$ are obtained for the respective energies within the constraints of the zero-temperature limit. From the simulated time evolution of the equipartition ratios ϵ plotted in Figure 2*d*, these growth rates are well reproduced (ϵ contains the squared field quantities). In conclusion, in the present study the cold plasma limit holds for all the simulations. $T_\perp$ remains in the sub-keV range for the entire linear regime. Significant thermal modifications, i.e., mode damping and the narrowing of the bandwidth of unstable wave numbers, is expected for less pronounced Δ_T only, which is the case if $T_\perp$ reaches at least a percentage of the collision bulk momentum. In contrast to fast-ignitor conditions, X-ray observations of early afterglows indicate rather moderate thermal cutoffs $\sim$5 keV. Hence, the initial scenario of cold plasma shells appears sensible. However, kinetic effects might become important for colliding shells of extremely unbalanced density ratios, i.e., for afterglow scenarios with a strong beam passing a rarefied interstellar cavity. Such scenarios are possible subjects for future studies.

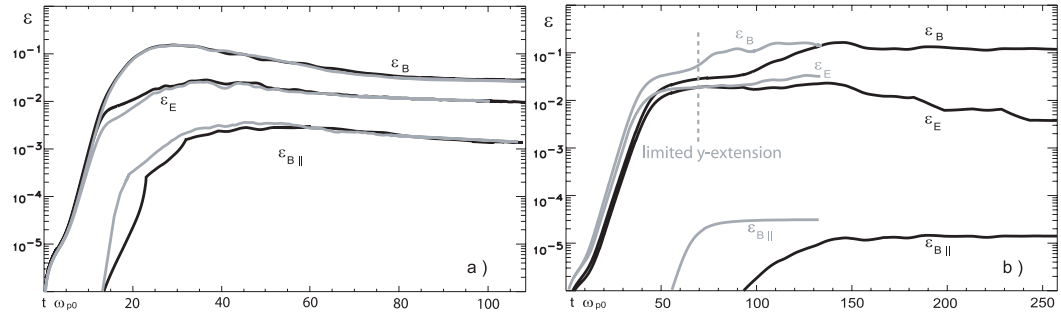

FIG. 3.—(*a*) Comparison of the equipartition ratios for simulations 1 and 2 (*gray*), which differ solely in initial $T_\perp$. Results are comparable in all essential quantities. In the linear regime, the growth rates are obtained as expected from the linear analysis in the cold beam limit. Saturated field values scale $\propto 1/(1 - v_{\rm th,\perp}^{\rm cms})$ (Silva et al. 2003), and hence thermal effects are insignificant during nonlinear saturation as well. In (*b*), ϵ evolutions are shown for simulations 3 and 4. Within the linear regime, results are again comparable, clearly indicating that dimensional effects are not modified by the finite size of the computational domain. Thus, the final steady state is reached earlier in simulation 4 (*gray*), coincidental with the transversal growth of the current self-pinches reaching the reduced *y*-extension of the system.

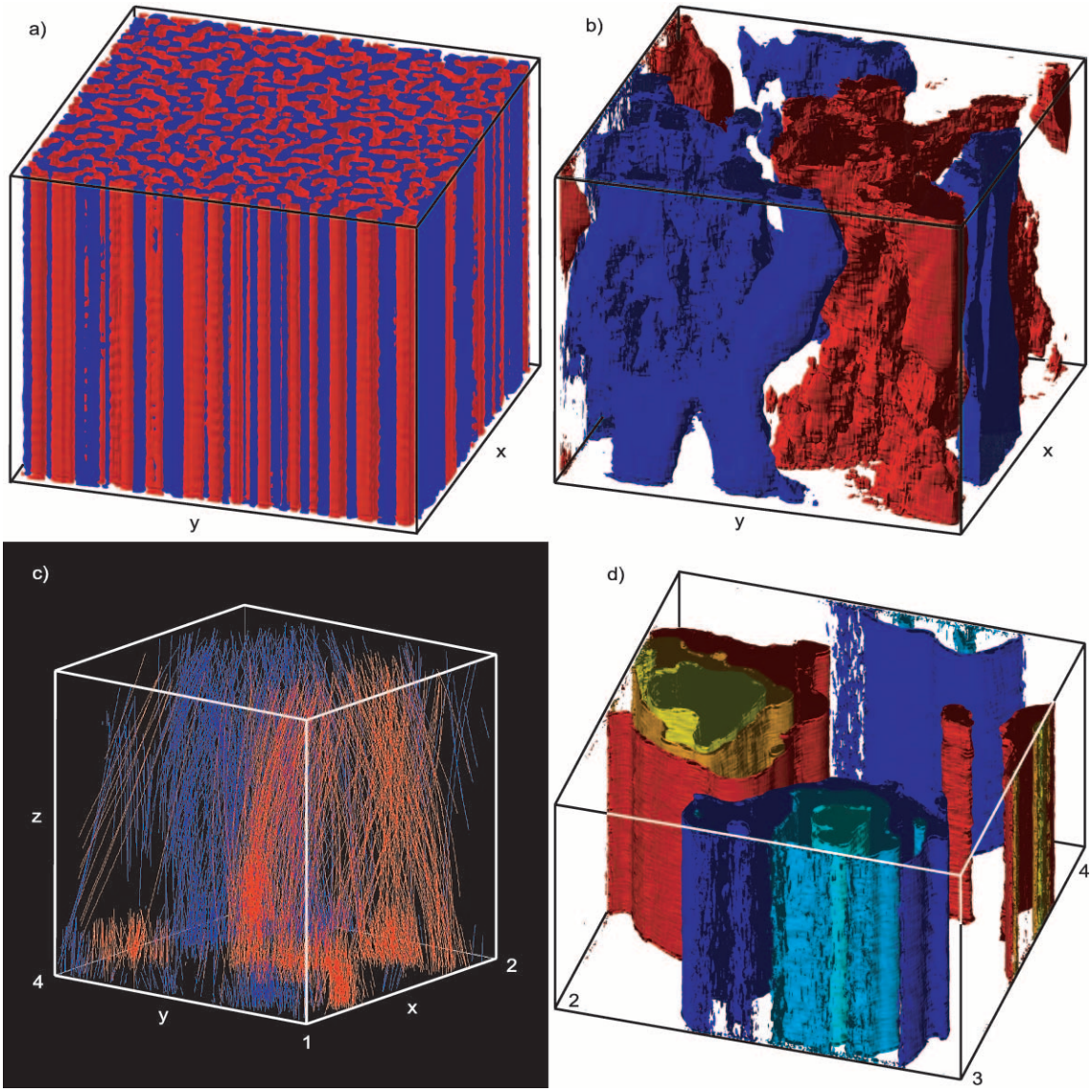

FIG. 4.—Isocontours of the current density in the saturated self-pinched state at (*a*) $t\omega_{p0} = 27$ ($j_z = \pm 0.75$) and (*b*) the final coalesced state $t\omega_{p0} = 250$ ($j_z = \pm 1.5$) for γ_0^{10}, with +*z*-directed currents in blue. Individual traces of 2048 selected positrons (*blue*) and electrons appendant to the +*z*-moving shell are shown in (*c*) for γ_0^{100} at $t\omega_{p0} = 250$. Particles perform a meandering motion in the magnetic void of each current filament. Directly corresponding are the respective current isocontours for $j_z = 4.5, 2.5,$ and 1.5 (*yellow, orange, and red*) and $j_z = -4.5, -2.5, -1.5$ (*turquoise, blue, and dark blue*) in (*d*). The relativistic dimensional reduction from three-dimensional to two-dimensional is obvious in the comparison of (*b*) and (*d*).

3.3. *The Saturated and Steady State Final Magnetic Fields*

The achievable equipartition ratio ϵ_B provided by the Weibel instability as the microphysical source process is an essential input quantity for global GRB synchrotron models. In the previous sections, the analysis was restricted to the linear regime, which is the first of three consecutive stages in the evolution of the instability. The linear state is followed by the intermediate stage of nonlinear saturation of the Weibel-generated magnetic fields in the maximum self-pinched state of current filamentation. The time scheme is finalized in a steady state configuration after neighboring filaments of aligned currents have merged. On astrophysical (=synchrotron loss) timescales, this last stage is the only one that is relevant. Kinetic simulations are the method of choice to obtain reliable values for the steady state ϵ_B rates. Figure 2*d* shows the time evolution of the transverse $\epsilon_{B\perp} = V^{-1}\int dV(B_x^2 + B_y^2)/8\pi\mu_{\rm kin}$ and longitudinal $\epsilon_{B\parallel} = V^{-1}\int dV B_z^2/8\pi\mu_{\rm kin}$ magnetic (WBI) fields. Since $\epsilon_{B\parallel}$ ratios (i.e., three-dimensional magnetic topologies) are negligible, $\epsilon_{B\perp} \simeq \epsilon_B$ and transverse magnetic fields are pervasive. Electric fields $E_\parallel$ and $E_\perp$ contribute about equal shares to the equipartition ratio, $\epsilon_E = V^{-1}\int dV(E_z^2 + E_\perp^2)/8\pi\mu_{\rm kin}$. Here $\mu_{\rm kin} = 4(\gamma_0 - 1)n_0mc^2$ is the initial kinetic energy density of the system. In the linear regime, ϵ_B and ϵ_E evolve in close proximity, i.e., the two-dimensional CTW mode dominates. Growth rates scale $\propto \gamma_0^{-1/2}$ and are quantitatively in very good agreement with linear theory, as has been described in § 3.1. Nonlinear saturation of the fields occurs in the maximum self-pinched state. Figure 4*a* illustrates that the closest-packed current self-pinches at the saturation point for γ_0^{10}. For the weakly relativistic cases, the current response to the self-pinching by the toroidal magnetic field is channeled into a velocity response $\delta\boldsymbol{j} \sim n_0\delta\boldsymbol{v}$. Beyond $\gamma_0 \sim 5$, this transforms into a density response $\delta\boldsymbol{j} \sim \delta n\boldsymbol{c}$, i.e., the density fluctuations increase toward higher collision energies, reaching up to $12n_0$ for γ_0^{100}. Each self-pinch consists of a void in the magnetic field enclosed by toroidal field walls.

Particles initially moving in $\pm z$ perform a meandering motion within each pinch, being reflected by the fields, with inverted directions at opposite walls as seen in Figure 4*c* (for better visibility, particle trajectories are shown here for a later phase). The saturated field values scale as $B_{\rm sat} \propto (n\gamma_0)^{1/2}/(1 - v_{\rm th})$, with saturation taking place when the meandering frequency $\omega_m \propto B\gamma_0^{-1}$ equals the CTW growth rate $\Gamma_{\rm CTW} \propto (n/\gamma_0)^{1/2}$. Obviously, thermal corrections to the saturated field $B_{\rm sat} \propto (1 - v_{\rm th}^{\rm cms})$ (Silva et al. 2003) become insignificant for sufficiently cold plasma shells. Silva et al. (2003) set the initial thermal spread to $v_{{\rm th},\perp}^{\rm cms} = 0.01$ for γ_0^{10}. The saturated field values obtained by them are in agreement with the values obtained in simulations 1 and 2, confirming that the cold beam approximation holds for all these simulations and that thermal corrections are negligible. Differences in the equipartition ratios are the sole result of the energy-dependent dimensional effects on which we focus in the present study. In contrast to the linear regime in which thermal corrections become more restrictive for higher collision energy (cf. § 3.2), the behavior of the CTW is modified during nonlinear saturation. In this phase thermal corrections are introduced via the velocity response, but since in the ultrarelativistic limit the density response δn dominates during pinching, thermal corrections become increasingly less important. In simulations 1 and 3 (Fig. 2*d*), the saturated $\epsilon_B^{\rm sat}$-values are equal for cases γ_0^{10} and γ^{100}. What differs are the coupling strength and the relative weight of the contributions from the TSI ($=\epsilon_{E\|}$) and WBI ($=\epsilon_{B\perp}$) modes in the nonlinear regime at later times: in the final phase, the current self-pinches coalesce. The magnetic fields around each self-pinched filament are practically at equipartition. The ''filling factor'' of the volume with self-pinches determines the final steady state ϵ_B.

The TSI imposes a complex three-dimensional structure on the current filaments for γ_0^{10} (Fig. 4*b*), thereby reducing the filling factor. Field energy is reconverted into disordered particle kinetic energy, causing particle heating. In Figure 2*d*, $\epsilon_{B\perp(E\|)}^{10}$ drops by 1 order of magnitude from the saturated to the final state. In contrast, for γ_0^{100} three-dimensional modifications of the final current/field configuration by the TSI are only marginal (Fig. 4*d*), whereas WBI contributions dominate. The reconversion process of energy is practically absent and $\epsilon_{B\perp}^{\rm sat} \sim \epsilon_{B\perp}^{\rm Bnal}$. The reconversion of (latent) field into (thermal) particle energy during the transition from nonlinear saturation to a final coalesced steady state is directly observable in the particle distribution functions shown in Figure 5. The comparative electrostatic energy excess for γ_0^{10} at decoupling time ($\epsilon_{E\|}^{10} \sim 10\epsilon_{E\|}^{100}$) is reconverted into particle kinetic energy, as seen in Figure 5*b*. Particles are accelerated in this case by the TSI up to 3.5 times the initial collision energy. For γ_0^{100}, particle heating and TSI are both suppressed; in contrast, WBI contributions and particle cooling are more pronounced (Fig. 5*a*). In conclusion, dimensional reduction in the ultrarelativistic regime is accompanied by an optimized conversion of particle free energy into magnetic field energy, i.e., optimized magnetic equipartition ratios. A critical final question is whether the observed dimensional effects are modified by the finite size of the computational domain. In view of this effect we varied the geometry of the simulation box between simulations 3 and 4, extending the parallel and one perpendicular dimension by a factor of 4 (Table 1). For the regimes of linear growth and nonlinear saturation, both simulations yield exactly the same results: according to Figure 3*b*, linear growth rates $\Gamma_{\rm CTW}$, the relations between $\epsilon_B, \epsilon_{B\|}$, and ϵ_E (i.e., the relative weight of TSI and WBI contributions to the two-dimensional coupled mode), and the times when nonlinear saturation is reached (i.e., coupling strengths) are exactly in accord. Furthermore, direct correspondence is seen in the time evolution of temperatures and anisotropies (Figs. 2*a*–2*c*). The saturated and final steady state equipartition ratios are comparable, although the final configuration is reached earlier in simulation 4. Because of computational limitations, the extension of the (x, z)-plane in simulation 4 enforces a corresponding reduction in y down to $L_y = 3.2(c/\omega_{p0})$. In the linear regime, the coupled CTW mode is two-dimensional and the y-extension is insignificant. Hence, the correspondence of results between simulations 3 and 4 proves that the dimensional effects under study have not been affected by the limitations of the computational domain. The simulations are comparable as long as the cross sections of the toroidal current self-pinches fit into the (x, y)-plane (Fig. 6*a*) of the simulation. The coalescence of self-pinches to the final steady state in simulation 4 precipitates the corresponding phase in simulation 3 as soon as the self-pinch diameter becomes comparable to L_y and the system is confined to be quasi–two-dimensional within the (x, z)-plane (Fig. 6*b*). The equipartition ratios are determined by the filling factor of the volume by current filaments. The equipartition ratios of simulations 3 and 4 are quantitatively comparable (Figs. 2*d* and 3*b*), and so are the shapes of the current filaments in z, as seen in Figures 4*d* and 6*b*. Disruption of filaments in z as taking place for γ_0^{10} (Fig. 4*b*) are absent, independent of the finite extension of the simulation box. The comparison of simulations 3 and 4 serves in the first place as proof that in the present simulations the contributions of the longitudinal TSI are not suppressed by the finite box extension in z. Such a result is intuitive, since the argumentation in § 3.1 is based on the relativistic damping of growth rates (=timescales, not wavenumber cutoffs). Furthermore, system variations in the transverse extension are not critical, since the cross sections of the coalesced current filaments in the final steady state configuration are primarily determined by $T_\perp$. Since the temperatures/anisotropies Δ_T (Fig. 2*c*) in all simulations saturate before spatial restrictions come into play, the final equipartition ratios obtained are independent of the finite box extensions. According to Figure 2*c*, some finite $\Delta_T \sim 2-3$ remains in the final steady state configuration (Yang et al. 1993a, 1993b). This

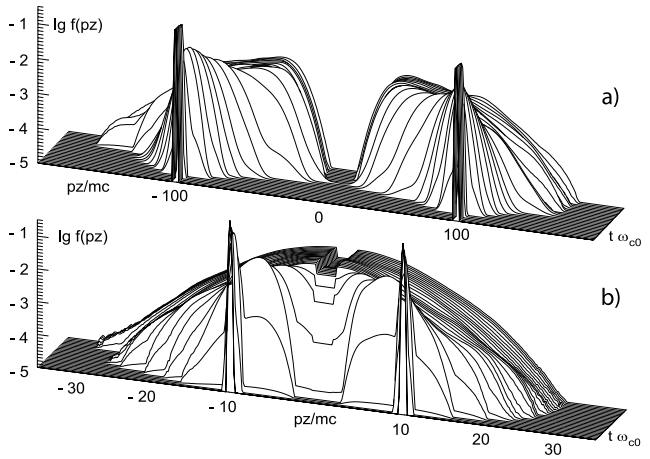

FIG. 5.—Time evolution of the normalized particle distributions $f(p_z)$ as a function of the p_z momentum for (*a*) γ_0^{100} and (*b*) γ_0^{10}. Parallel electric fields $E_\|$ attributable to the electrostatic TSI contributions are more pronounced for lower energies. Consequently, particle acceleration is more prominent in (*b*) for γ_0^{10}, where $p_z/mc \sim \gamma$ reaches up to 3.5 times the initial bulk momentum/relativistic energy γ_0.

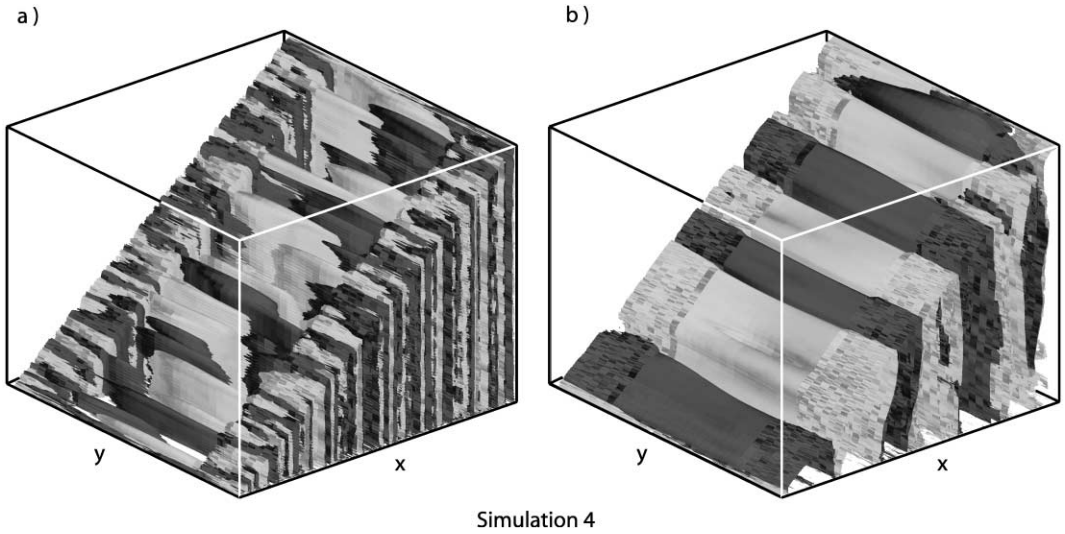

FIG. 6.—Isocontours of the current ($j > 0$, *black*) in (*a*) the phase of nonlinear saturation at $t\omega_{p0} = 48$ and (*b*) after extending beyond the *y*-extension of the system at $t\omega_{p0} = 100$, which in simulation 4 is reduced to $L_y = 3.2(c/\omega_{p0})$. In (*b*), the configuration is reduced to quasi two-dimensional, artificially stretched ad infinitum in *y*. Consequences on the field structure are comparable to those of the coalescence of current self-pinches at later times. Therefore, the time evolution is shifted and the final steady state equipartitions are comparable, but precipitate relative to simulation 3 as shown in Fig. 3*b*.

residual anisotropy is slightly higher in the ultrarelativistic regime. This fact sustains the essential statement of dimensional effects, in which WBI contributions/filamentation become gradually more pronounced at higher relativistic energies. The current filaments have a preferential direction and modifications in *z*-structure are reduced; as a consequence, residual anisotropies remain. In view of the emission of synchrotron radiation, an interesting factor is the time evolution of the pitch angles, $\cos\phi = \boldsymbol{B}\cdot\boldsymbol{p}/Bp$, of the particles involved. Figure 7 shows that pitch-angle isotropization takes place most efficiently in the regime following nonlinear saturation during the final coalescence of self-pinches. Because of inertial effects on the particles the pitch angles isotropize later for higher than for lower energies, γ_0. However, even for the external high collision energies between the shells, the pitch angle isotropization takes place and is complete on timescales that are short compared with typical synchrotron loss times.

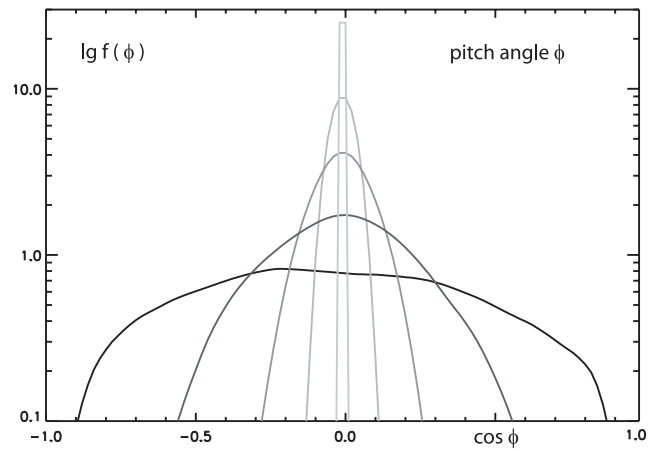

FIG. 7.—Isotropization of synchrotron pitch angles for simulation 3 as time cascade $t\omega_{p0} = 5, 75, 94, 112, 245$ (*darkening from light gray to black*). Apparently, isotropization is pervasive in the nonlinear regime and takes place most efficiently after equipartitions are at maximum (i.e., for γ_0^{100} after $t\omega_{p0} \sim 100$). Within the total simulated time, i.e., on a timescale that is negligible with respect to typical synchrotron loss times, practically complete isotropy is reached.

4. SUMMARY AND PERSPECTIVES

We have presented self-consistent, fully electromagnetic three-dimensional PIC simulations of electron-positron plasma shell collisions at moderately relativistic to ultrarelativistic collision energies, γ_0^{10} and γ_0^{100}, with total particle ensembles of $\sim 5 \times 10^8$. For the first time, the generation of magnetic fields by the Weibel instability has been investigated for external collision energies of $\gamma_0 \sim 100$. As a peculiarity of this energy regime, we find that three-dimensional modifications by the TSI mode become progressively insignificant. As a consequence, the conversion of particle kinetic energy into magnetic fields by the Weibel mechanism takes place with optimized efficiency in quasi–two-dimensional shell slices. We provided evidence that such dimensional effects are introduced in the ultrarelativistic regime by the damping of TSI contributions to the two-dimensional coupled two-stream Weibel mode and are not influenced by variations of the computational domain. We provided arguments from linear theory for this transition that turn out to hold in the highly nonlinear late-time evolution covered by the PIC simulations. From the reduction of dimensionality, final steady state equipartition ratios of $\epsilon_B \sim 12.5\%$ result for external collision energies, exceeding the respective values achieved in internal collisions by a factor of 5. The linear analysis was performed within the constraints of the cold beam limit (zero-temperature approximation). This assumption is valid as long as the thermal spread of plasma shells is less then 1% of the bulk collision energy. In this respect, the scenario under study is fundamentally different from fast-ignitor scenarios. We have demonstrated that dimensional effects are introduced as new physical behavior in the ultrarelativistic regime. For the cold initial temperatures at hand, such a behavior is not affected by kinetic effects as far as linear kinetic analysis is concerned. The phenomenon of dimensional reduction was not included in previous studies of the highly nonlinear late-time evolution, which are either lower dimensional or different in the energy regime. We note that for

the external collision of GRB fireball ejecta with the surrounding medium, contributions from electron-proton plasma (Nishikawa et al. 2003) are also involved. As has been noted by Silva et al. (2003), the fundamental instability process/ϵ_B-values will remain unchanged in this case; only the time and length scales are upscaled by the proton-to-electron mass ratio $(m_p/m)^{1/2} \sim 43$. The critical question is, however, the lifetime of the final steady state magnetic fields in this case, since typical synchrotron loss times range in the order of 10^5 times the total simulated time. The dominant process responsible for the decay of the magnetic fields in this case is collisionless diffusion. Typical decay rates and diffusion coefficients obtained from self-consistent PIC simulations will be presented elsewhere (Jaroschek et al. 2004).

The authors thank S. Matsukiyo, K. Hallatschek, and M. Scholer for fruitful discussions, and the Computing Center of the Max-Planck-Society in Garching and the Leibniz Computing Center in Munich for the granted computation time. The work of C. H. J. was performed under the auspices of the International Max-Planck Research School on Astrophysics.

REFERENCES

Birdsall, C. K., & Langdon, A. B. 1991, Plasma Physics via Computer Simulation (Bristol: IOP)
Califano, F., Pegoraro, F., & Bulanov, S. V. 1997, Phys. Rev. E, 56, 963
de Groot, S. G., Leeuwen, W. A., & van Weert, C. G. 1980, Relativistic Kinetic Theory (Amsterdam: North-Holland)
Gruzinov, A. 2001, ApJ, 563, L15
Haruki, T., & Sakai, J. I. 2003, Phys. Plasmas, 10, 392
Jaroschek, C. H., Lesch, H., & Treumann, R. A. 2004, ApJ, 606, 1065
Kazimura, Y., Sakai, J. I., Neubert, T., & Bulanov, S. V. 1998, ApJ, 498, L183
Lee, R., & Lampe, M. 1973, Phys. Rev. Lett., 31, 1390
Medvedev, M. V, & Loeb, A. 1999, ApJ, 526, 697
Meszaros, P. 2002, ARA&A, 40, 137
Nishikawa, K. I., Hardee, P., Richardson, G., Preece, R., Sol, H., & Fishman, G. J. 2003, ApJ, 595, 555
Panaitescu, A., & Kumar, P. 2002, ApJ, 571, 779
Piran, T. 1999, Phys. Rep., 314, 575
Pruet, J., Abazajian, K., & Fuller, G. 2001, Phys. Rev. D, 64, 063002
Sagdeev, R. Z. 1966, Rev. Plasma Phys., 4, 23
Saito, S., & Sakai, J. I. 2004, Phys. Plasmas, 11, 859
Silva, L. O., Fonseca, R. A., Tonge, J. W., Dawson, J. M., & Mori, W. B. 2003, ApJ, 596, L121
Silva, L. O., et al. 2002, Phys. Plasmas, 9, 2458
Weibel, E. S. 1959, Phys. Rev. Lett., 2, 83
Yang, T.-Y. B., Arons, J., & Langdon, A. B. 1993a, Phys. Fluids B, 5, 3059
Yang, T.-Y. B., Gallant, Y., Arons, J., & Langdon, A. B. 1993b, Phys. Fluids B, 5, 3369
Yoon, P. H. 1989, Phys. Fluids B, 1, 1336
Yoon, P. H., & Davidson, R. C. 1987a, Phys. Rev. A, 35, 2619
———. 1987b, Phys. Rev. A, 35, 2718